Available online at www.sciencedirect.com
ScienceDirect
Trans. Nonferrous Met. Soc. China 34(2024) 1774−1788
Transactions of Nonferrous Metals Society of China
www.tnmsc.cn

Effect of pre-deformation on microstructure and mechanical properties of 2050 Al−Li alloy

Yao LI[1], Guo-fu XU[1,2], Hai-guang QIAO[1], Shi-chao LIU[1], Xiao-yan PENG[1]

1. School of Materials Science and Engineering, Central South University, Changsha 410083, China;
2. Key Laboratory of Nonferrous Metal Materials Science and Engineering, Ministry of Education, Central South University, Changsha 410083, China

Received 25 December 2022; accepted 25 July 2023

Abstract: The microstructural evolution and mechanical properties of 2050 Al−Li alloy subjected to different rolling pre-strains (0−20%) and aging (T8) were studied. Transmission electron microscopy (TEM) and scanning electron microscopy (SEM) were used to characterize the microstructure. The results show that the grains were significantly refined along the normal direction (ND) and the intragranular distortion increased with the increase of pre-strain level. The entanglement of defects, e.g., dislocations, provides a large number of nucleation sites for the precipitation of T_1 phases. This leads to larger number of precipitates and narrower distance between precipitates, thus improving the hindering effects on dislocation motions and the strength of the alloy. When the pre-deformation level reaches 16%, the alloy shows the highest density of T_1 phases and strength (the yield strength and tensile strength reach 568 and 584 MPa, respectively, and elongation is 8.6%). When the amount of pre-deformation is further increased to 20%, the atomic diffusion channels are reduced due to dislocation entanglement, and the reduction in the number of T_1 phases eventually leads to a decrease in strength of the alloy.

Key words: 2050 Al−Li alloy; rolling pre-deformation; T_1 phase; microstructure; mechanical properties

1 Introduction

Al−Li alloys serve as key industrial structural materials with many advantages such as low density, high strength, low temperature toughness, good corrosion resistance and plastic formability. They have been widely used in the aerospace, transportation, weapons, ships, and many other industries [1]. According to Refs. [2,3], for every 1% of Li element added to Al alloy, the mass of Al alloy can be reduced by 3%, and the elastic modulus can be increased by 6%. Therefore, many efforts have been made to modify the microstructure and enhance the mechanical properties of Al−Li alloys, such as optimizing the alloy composition, changing the forming method, and adjusting the heat treatment system. Compared with the previous Al−Li alloy, the third-generation Al−Li alloys show higher strength, better toughness, and lower anisotropy due to their higher Cu/Li ratio [4,5]. Among them, 2050 Al−Li alloy has been used as the main structural material of aircraft skins and rockets due to its high strength, excellent rigidity and good welding performance [6]. Its superior mechanical performance can be originated from several precipitated phases including T_1 (Al_2CuLi), δ'(Al_3Li) and θ'(Al_2Cu) [7]. SHAMRAI et al [8] discovered that T_1 phase plays the major role in precipitation strengthening of 2050 Al−Li alloy. The precipitation of T_1 phase mainly occurs at subgrain boundaries and intragranular defects. The

Corresponding author: Xiao-yan PENG, Tel: +86-15111032048, E-mail: pxy0807@126.com
DOI: 10.1016/S1003-6326(24)66506-4

strong hindrance of T_1 phase to dislocation movement is the main reason for the alloy strength enhancement [9−11].

The deformation before the aging process (pre-deformation) can influence the precipitation behavior [12] and thus influence the mechanical performance. CASSADA et al [13] discovered that pre-deformation can promote the aging precipitation process of the T_1 phase, because a large number of defects such as vacancies and dislocations will be generated in the Al matrix. As heterogeneous nucleation sites for T_1 phase, dislocations can serve as a rapid diffusion channel for solute atoms during the aging process. Therefore, dislocations can promote the nucleation and growth of the T_1 phase. XIE et al [14] studied the effect of pre-deformation on the microstructure and properties of the 2195 Al alloy, and found that pre-deformation can effectively inhibit the formation of Cu atom clusters, thereby promoting the precipitation of T_1 phase, and finally improving the mechanical properties. DUAN et al [15] studied the effects of rolling pre-deformation on the microstructure and mechanical properties of Al−Cu−Li alloys. They found that the nucleation and precipitation of the T_1 phase were greatly promoted after the alloy was subjected to rolling pre-deformation treatment, at the same time, the precipitation of other phases was inhibited. However, in most studies, the pre-deformation strains were less than 10%, and high pre-strain levels have rarely been explored. Meanwhile, many studies reported that the strength increases monotonically with the increase of pre-deformation, the question that if the strength can be further enhanced at high pre-strain levels still remains unanswered. In addition, the role of pre-deformation in influencing the precipitation behavior, grain structure and resultant mechanical properties still remains unclear, which also needs to be thoroughly investigated.

Therefore, in this work, different rolling pre-strains (0, 4%, 8%, 12%, 16%, and 20%) were introduced before aging. The evolution of mechanical properties and microstructures, such as precipitation behavior and dislocations, with the change of pre-strain, was revealed in detail. The role of pre-strain in promoting precipitation and enhancing mechanical properties was also discussed.

2 Experimental

2.1 Materials processing

The chemical composition of the pre-deformed 2050 Al−Li alloy from a domestic company was Al−3.67Cu−1.0Li−0.44Mg−0.44Ag−0.37Mn−0.10Zr−0.10Ti−0.25Zn (wt.%). The 27 mm-thick plate was annealed at 525 °C for 4 h and hot-rolled into a 5 mm thin plate. The hot-rolled sheets were annealed at 500 °C for 2 h, and then the plate was cold rolled to a thickness of 2 mm at room temperature. The cold-rolled sheet was subjected to solution treatment at 520 °C for 1 h, water quenched to room temperature and then pre-deformed at strains of 0, 4%, 8%, 12%, 16% and 20% on the rolling machine. After the pre-deformation, the samples were subjected to an aging heat treatment at 150 °C for 40 h (T8).

2.2 Hardness test

To study the influence of pre-deformation on hardening, the sample after aging treatment was polished with 600# sandpaper first, and then 1000#, 1500# and 2000# sandpapers were used to refine the scratches. Finally, the sample was polished till the absence of scratches. The sample was tested with a Vickers hardness tester, the loading force was 1 kg, and the loading time was 15 s. Five different positions were selected for each sample and the hardness average value was taken.

2.3 Tensile test

The mechanical properties of the samples after aging treatment were tested by the AG-X plus electronic universal tensile testing machine. The wire cutting machine was used to cut the aged standard tensile specimen, as shown in Fig. 1. The stretching direction of the tensile sample was parallel to the rolling direction, and the tensile rate was 2 mm/min. For each sample with different pre-deformations, three parallel samples were tested

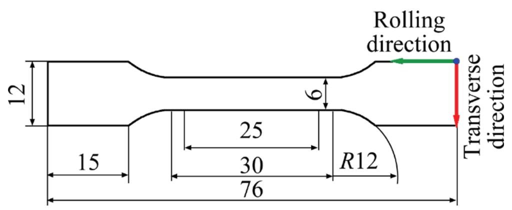

Fig. 1 Geometry of tensile specimen (unit: mm)

to obtain the average value of the tensile strength (σ_b), yield strength (σ_s) and elongation.

2.4 Microstructural characterization

Fractured samples were observed using a Sirion 200 scanning electron microscope (SEM), operating at 15 kV. The grain morphologies after different pre-deformation treatments were observed by electron backscattered diffraction (EBSD), performed on a Sirion field emission scanning electron microscope with an electron backscattered diffractometer probe. Experimental data were analyzed using a TSL OIM software. After mechanical polishing, EBSD samples were electrolyzed and polished. The electrolytic polishing solution was a mixture of ethanol and perchloric acid with a volume ratio of 9:1. The polishing voltage was 12 V and the polishing temperature was controlled below −20 °C.

To observe the precipitation characteristics of aging samples after different pre-deformation treatments, a Tecnai G2 20ST transmission electron microscope (TEM) was used, performing at 200 kV. Before TEM observation, the sample was ground to a thickness of about 80 μm, and then double-spray electrolyzed in the electrolyte containing 70 vol.% methanol and 30 vol.% nitric acid at −20 °C.

3 Results

3.1 Mechanical properties

Figure 2 shows the mechanical properties of the T8-aged alloys subjected to different pre-strains (0, 4%, 8%, 12%, 16%, and 20%). With the increase of pre-strain, the σ_s and σ_b first increase and then decrease, while the elongation keeps decreasing. The undeformed sample showed the minimum σ_s and σ_b of 428 and 451 MPa, respectively, with the maximum elongation of 14.6%. When the pre-strain increases to 16%, the sample reaches the highest strength (σ_s=568 MPa, σ_b=584 MPa), while maintains good ductility with elongation of 8.6%.

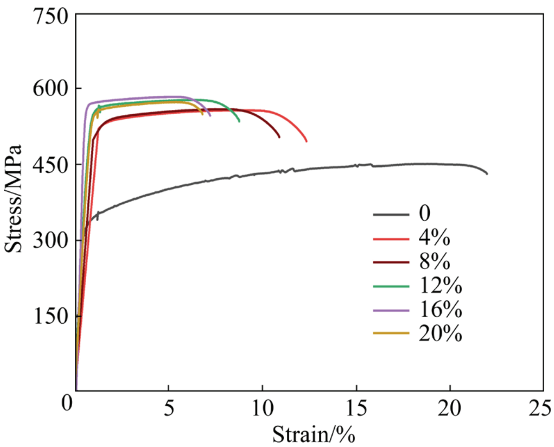

Fig. 2 Tensile mechanical properties of 2050 Al−Li alloy with different pre-deformations after T8 aging treatment

3.2 Fracture morphology

Figure 3 shows tensile fracture morphologies of the alloys after pre-deformed to different strain levels and aging treatment. The fracture mode of the alloys is mainly transgranular dimple fracture, and with the increase of pre-strain, the number of dimples gradually decreases. The fracture morphology of the undeformed sample mainly consists of uniform dimples as shown in Fig. 3(a). With the increase of the pre-strains, the fracture cracks on the fracture surface gradually increase, and the number of dimples gradually decreases. For example, when the pre-strain increases to 8%, several fracture cracks can be observed (Fig. 3(c)).

3.3 Microstructure characterization

Figure 4 shows the electron backscattered diffraction (EBSD) patterns along the TD−ND plane of the 2050 Al−Li alloy after different pre-strain treatments. The high angle grain boundaries (HAGBs, with misorientation angle in the range of 15°−180°) and low angle grain boundaries (LAGBs, with misorientation angle in the range of 3°−15°), were marked by black and white lines, respectively. The grain size gradually decreases along the ND direction and the LAGB gradually increases with the increase of pre-strain.

Figure 5 shows the grain average mis-orientation (GAM) diagrams along the TD−ND plane of the solid solution 2050 Al−Li alloy treated with different pre-deformations. It can be seen that the GAM of the samples after pre-deformation locates in the range of 0−5. When the pre-strain is 0, the GAM is very small. With the gradual increase of the pre-strain, the average GAM increases significantly. The samples with pre-strains of 16% and 20% share a very similar average GAM of ~0.99.

Figure 6 shows the TEM dark field images of the T_1 phase along the ⟨112⟩ direction of the alloy subjected to different pre-strains and T8 aging

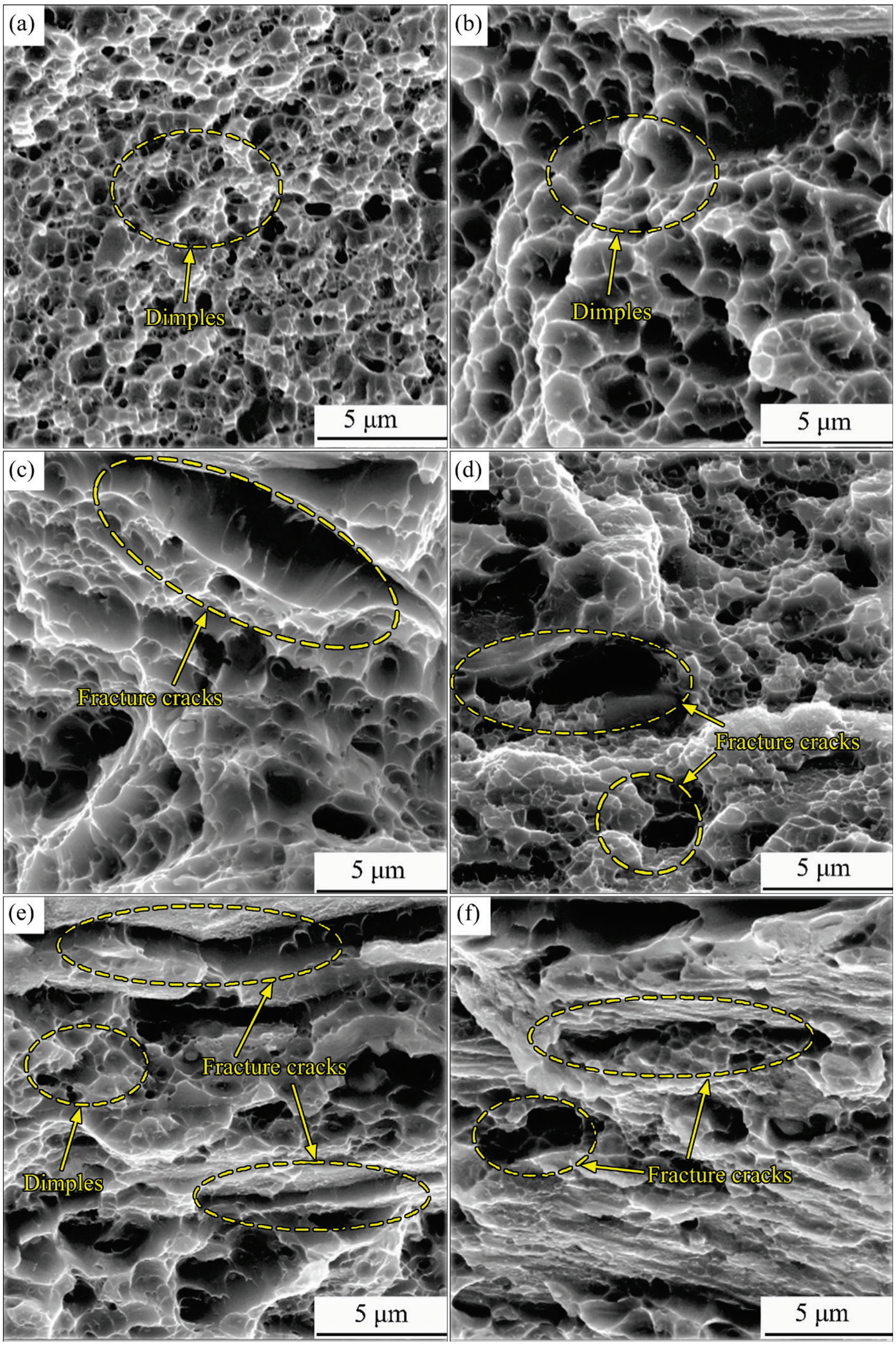

Fig. 3 Room temperature tensile fracture morphologies of 2050 Al−Li alloy subjected to different pre-deformations after T8 aging treatment: (a) 0; (b) 4%; (c) 8%; (d) 12%; (e) 16%; (f) 20%

treatment. Lath-like T_1 phases are the main strengthening phase of Al−Li alloys with high Cu/Li ratio [16], and they precipitated on the $\{111\}_\alpha$ surface and showed $(0001)_{T_1}//\{111\}_\alpha$ and $[10\bar{1}0]_{T_1}//[110]_\alpha$ orientation relationship with the matrix. As shown in Fig. 6(a), the T_1 phase in the undeformed sample showed very large diameter and thickness, but low density. With the increase of the pre-strain, the diameter and thickness of the T_1 phase gradually decreased, and the number density gradually increased. Compared with the sample with pre-strain of 16%, the T_1 phase in the sample with pre-strain of 20% showed a lower density and smaller diameter, but larger thickness.

Figure 7 shows the selected area diffraction patterns (SADPs) along the ⟨112⟩ direction of the 2050 Al−Li alloy with different pre-strains after T8 aging treatment. T_1 phase is the main precipitation phase. The orientation relationship between the T_1 phase and the Al matrix is $(0001)_{T_1}//(111)_{\mathrm{Al}}$,

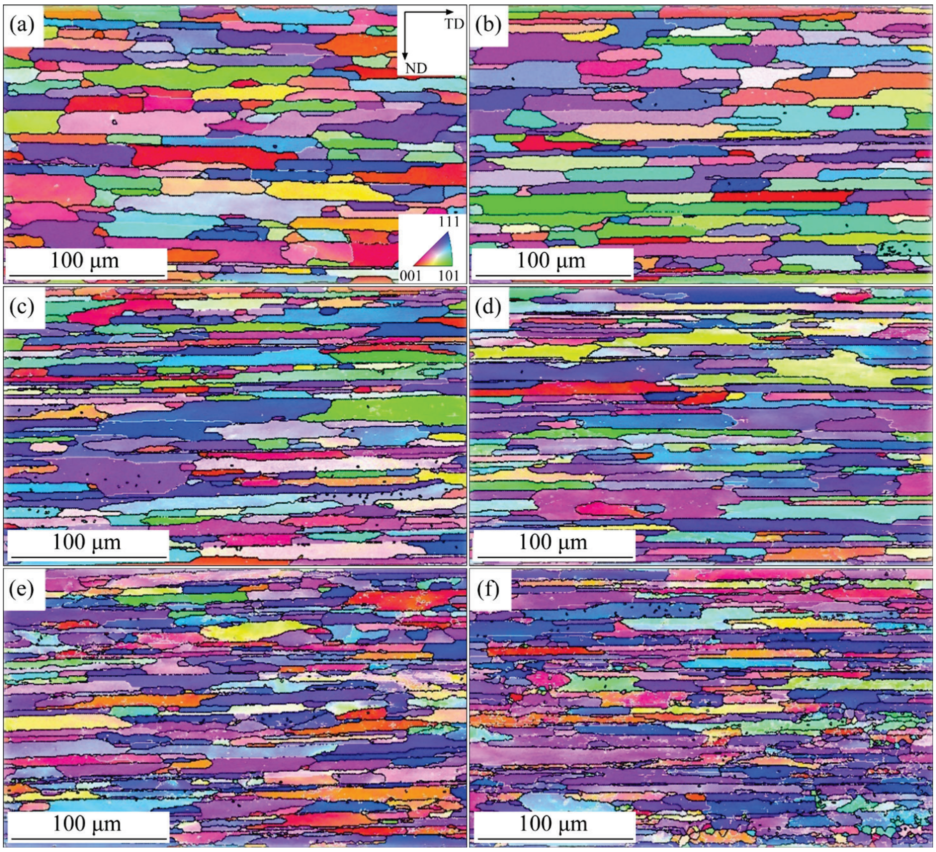

Fig. 4 EBSD diagrams of 2050 Al−Li alloy along TD−ND plane with different pre-deformations: (a) 0; (b) 4%; (c) 8%; (d) 12%; (e) 16%; (f) 20%

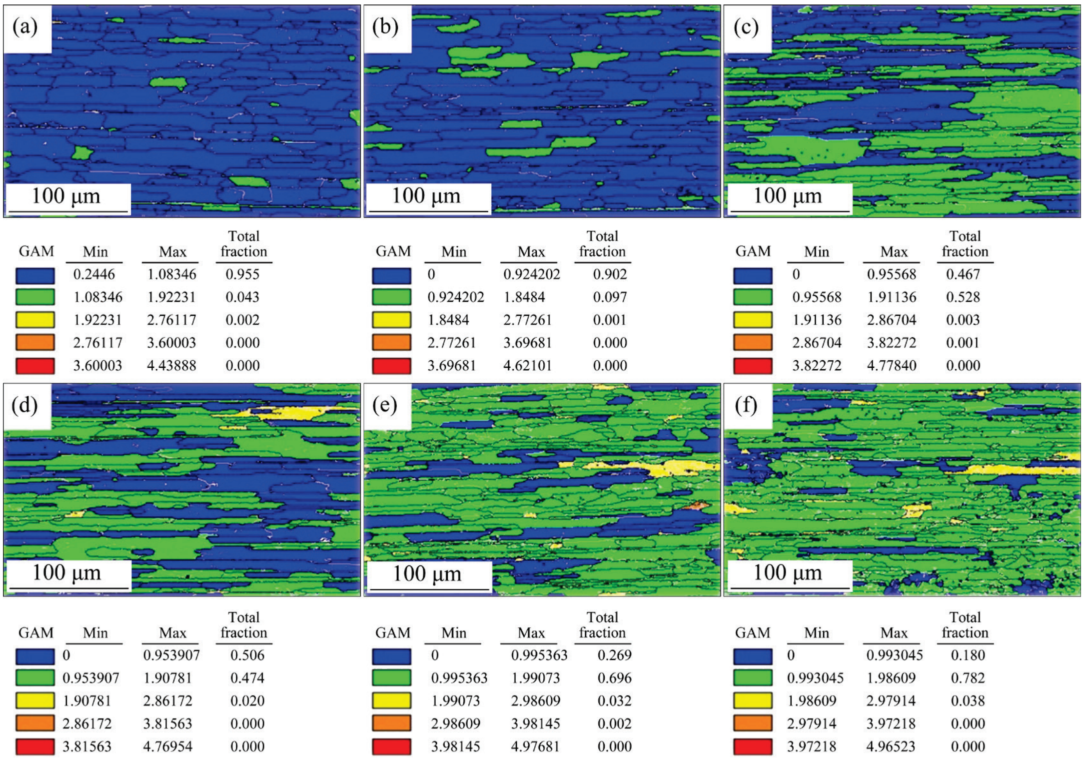

Fig. 5 GAM diagrams of 2050 Al−Li alloy along TD−ND plane with different pre-deformations: (a) 0; (b) 4%; (c) 8%; (d) 12%; (e) 16%; (f) 20%

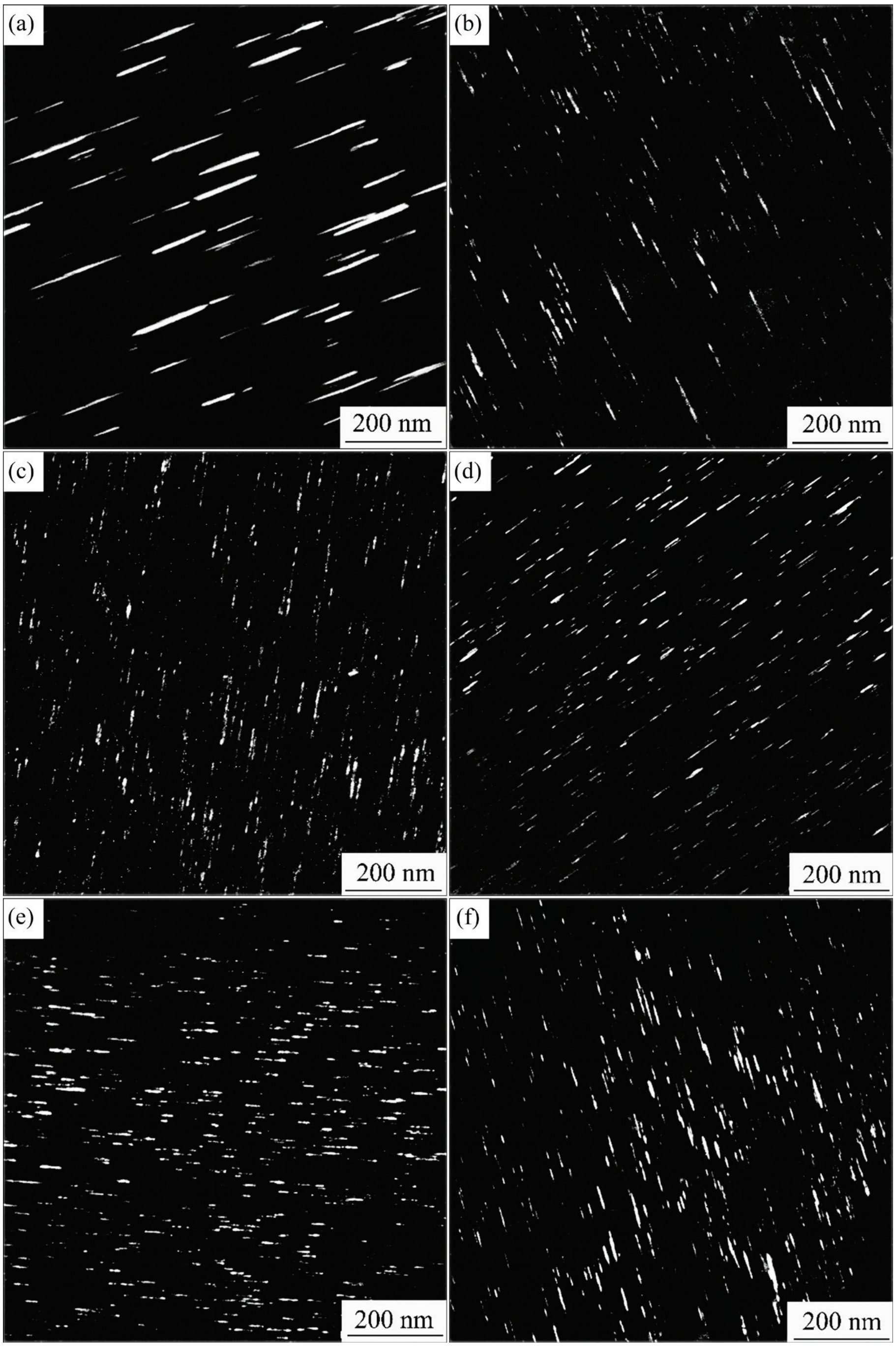

Fig. 6 TEM dark field images of T_1 phase along ⟨112⟩ direction of 2050 Al−Li alloy with different pre-deformations after T8 aging treatment: (a) 0; (b) 4%; (c) 8%; (d) 12%; (e) 16%; (f) 20%

$[120]_{T_1}//[211]_{Al}$, and $[1010]_{T_1}//[110]_{Al}$. With the increase of the pre-deformation strain, the intensity of the T_1 phase diffraction spots increased.

Figure 8 shows the TEM dark field images of the θ' phase along the ⟨100⟩ direction of the 2050 Al−Li alloy with different pre-strains after T8 aging treatment. The orientation between θ' phase and matrix is $(100)_{Al}//(100)_{\theta'}$ and $[001]_{Al}//[001]_{\theta'}$. When the pre-strain is small, the precipitate amount of the θ' phase gradually increases (Figs. 8(a, b)) with the increase of the pre-strain. When the pre-strain is not less than 8%, the amount of θ' phase precipitate gradually decreases with the increase of the pre-strain, as shown in Figs. 8(c−f).

Figure 9 shows the SADPs along the ⟨100⟩ direction of the 2050 Al−Li alloys with different pre-strains and after T8 aging treatment. The main precipitation phases are θ' phase and T_1 phase along ⟨100⟩ direction. However, when the pre-strain is greater than 4%, the intensity of the diffraction

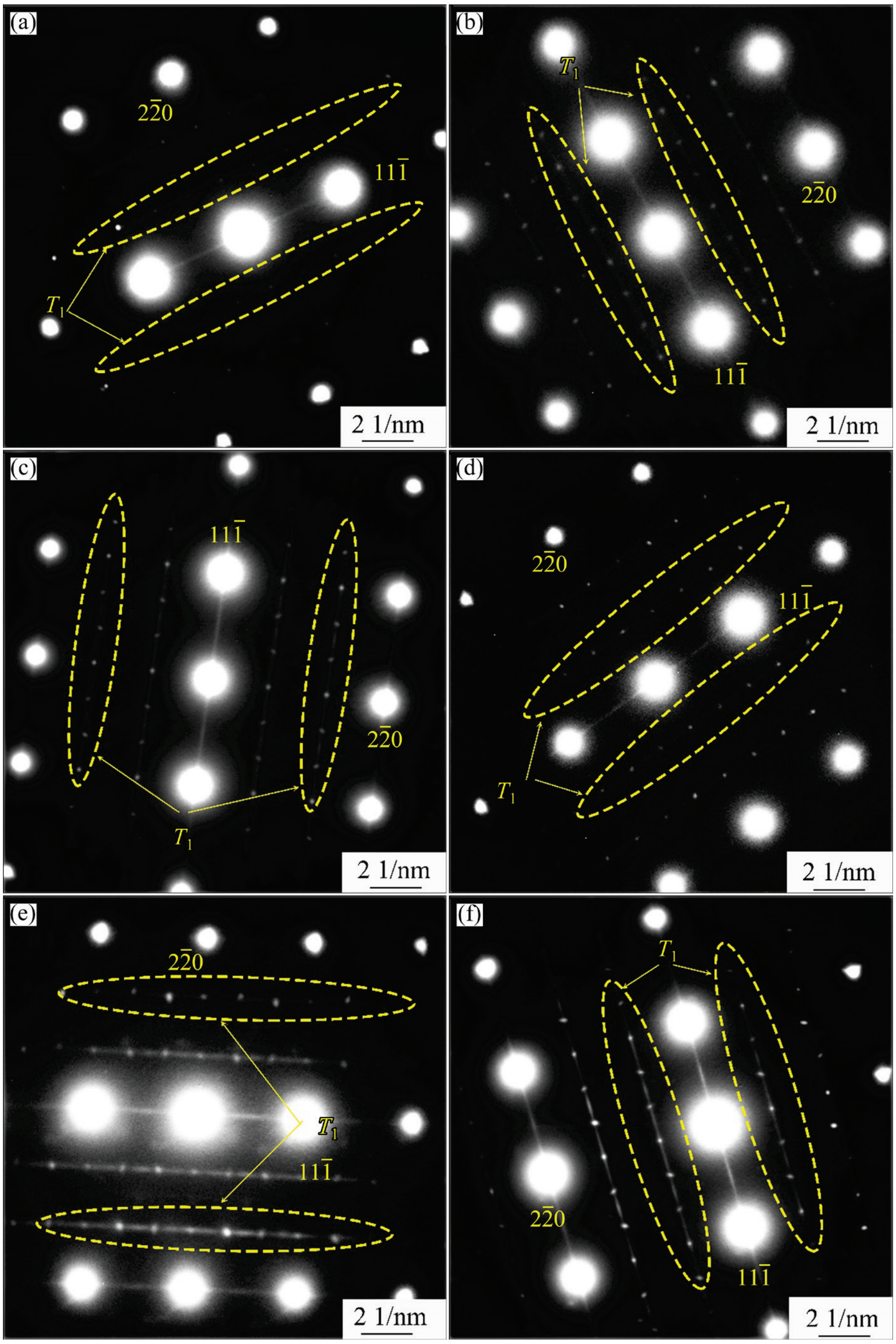

Fig. 7 SADPs along ⟨112⟩ direction of 2050 Al−Li alloy with different pre-deformation after T8 aging treatment: (a) 0; (b) 4%; (c) 8%; (d) 12%; (e) 16%; (f) 20%

pattern of the θ' phase gradually decreases. When the pre-strain reaches 16% and 20%, the sample shows the weakest the diffraction pattern, indicating that the quantity of the precipitated θ' phase reached the minimum among the tested samples.

In order to further calculate the sizes of the precipitates in the 2050 Al−Li alloy with different pre-strains and T8 aging, the Image-pro plus image processing software was used to measure the average diameter and density of the T_1 and θ' phases and the average thickness of the T_1 phase and the proportion of the T_1 phase sheared by dislocations, as shown in Fig. 10. According to Fig. 10(a), with the increase of pre-strain, the average diameter of T_1 strengthening phase continued to decrease, while the density of the precipitate continued to increase until the pre-strain reached 16%. The diameter of T_1 phase in the sample with pre-strain of 0 was 83.6 nm.

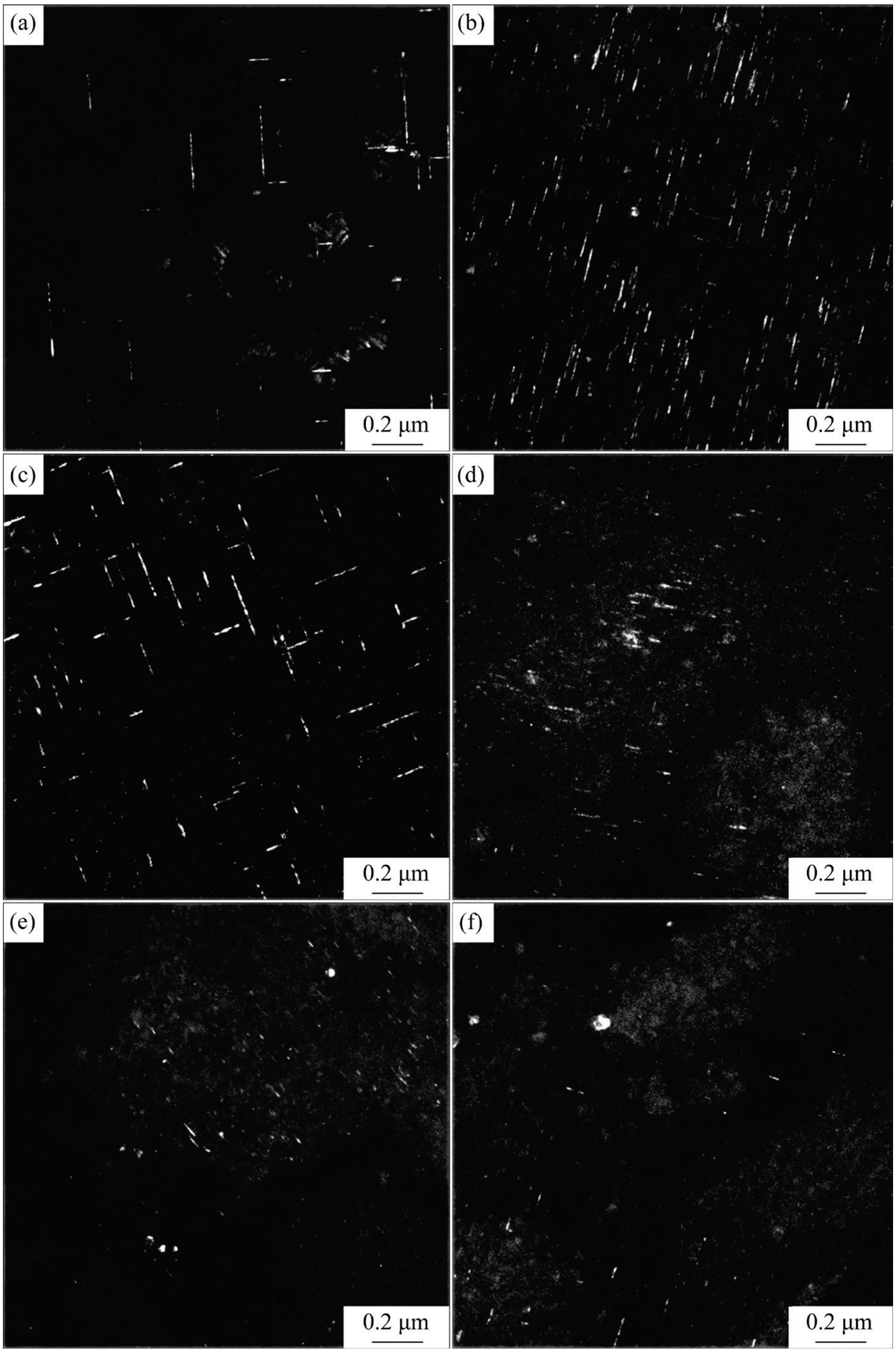

Fig. 8 TEM dark field images of θ' phase along ⟨100⟩ direction of 2050 Al−Li alloy with different pre-deformations after T8 aging treatment: (a) 0; (b) 4%; (c) 8%; (d) 12%; (e) 16%; (f) 20%

Compared with the sample without pre-deformation, the diameter of T_1 phase in the 4% sample sharply reduced. The diameters of T_1 precipitates in 4%, 8%, 12%, 16% and 20% samples are 31.4, 30.1, 28.8, 27.5 and 24.2 nm, respectively. In addition, the number density of T_1 precipitates in 4%, 8%, 12%, 16% and 20% samples were 636.8, 789.5, 954.5, 1166.4 and 1023.3 μm^{-2}, respectively. But for the sample without pre-deformation, the number density of the T_1 precipitates was only 110.3 μm^{-2}.

It can be seen from Fig. 10(b) that the average diameter of θ' strengthening phase gradually decreased with the increase of pre-deformation degree, while the number density first increased and then decreased. The diameters of θ' precipitates in 0, 4%, 8%, 12%, 16% and 20% samples were 93.2, 55.4, 47.2, 29.2, 24.5 and 23.1 nm, respectively.

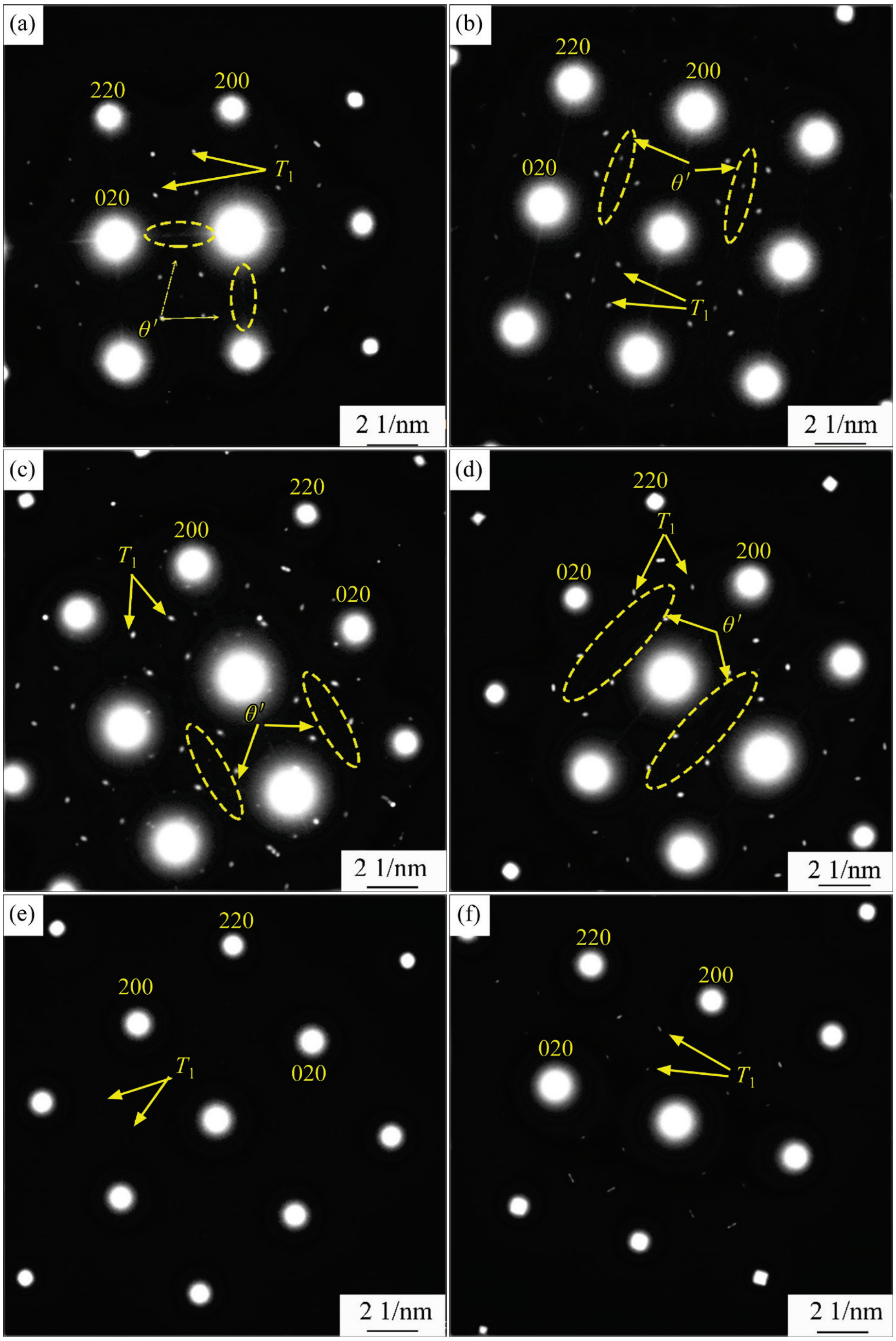

Fig. 9 SADPs along ⟨100⟩ direction of 2050 Al−Li alloy with different pre-deformations after T8 aging treatment: (a) 0; (b) 4%; (c) 8%; (d) 12%; (e) 16%; (f) 20%

The number densities of θ' precipitates in 0, 4%, 8%, 12%, 16% and 20% samples were 12.6, 112.1, 93.6, 54.4, 33.8 and 10.6 μm^{-2}, respectively.

It can be seen from Fig. 10(c) that the average thickness of the T_1 phase decreased gradually with the increase of pre-strain. When the pre-strain exceeds 16%, the average thickness of T_1 phase begins to increase. Studies [17] have shown that when the thickness of the T_1 phase is less than 3 nm, it can be sheared by dislocations, otherwise, dislocations can only bypass the T_1 phase. Therefore, as shown in Fig. 10(c), when the pre-strain is less than 16%, the number of T_1 phases sheared by dislocations gradually increases with the increase of the pre-strain. However, when the pre-strain reaches 20%, the proportion of sheared T_1 phase decreases, but it is still greater than 50%.

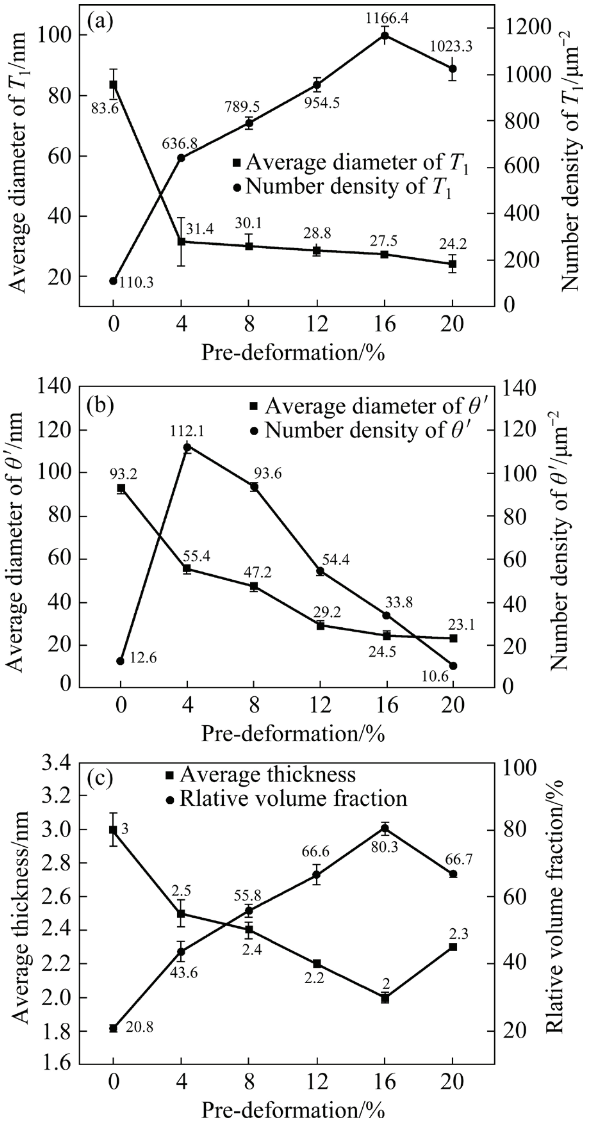

Fig. 10 Average diameter and number density of T_1 (a) and θ' (b) phase precipitates, and average thickness and relative volume fraction of T_1 phase (c) for different rolling samples

From Fig. 11, it is shown that the nucleation and precipitation of the T_1 phase near the dislocation distortion region and the T_1 phase (with thickness less than 3 nm) can be sheared by dislocations. It can be seen from Fig. 11(a) that during the pre-deformation, the matrix is obviously distorted due to the generation of dislocations. Near the distortion zone, there is obvious precipitation phenomenon of T_1 phase. Furthermore, when the size of the precipitate is less than 3 nm, it can be sheared by dislocations. When the T_1 phase is sheared by dislocations, the atomic arrangement of the T_1 phase is obviously dislocated, as shown in Fig. 11(b).

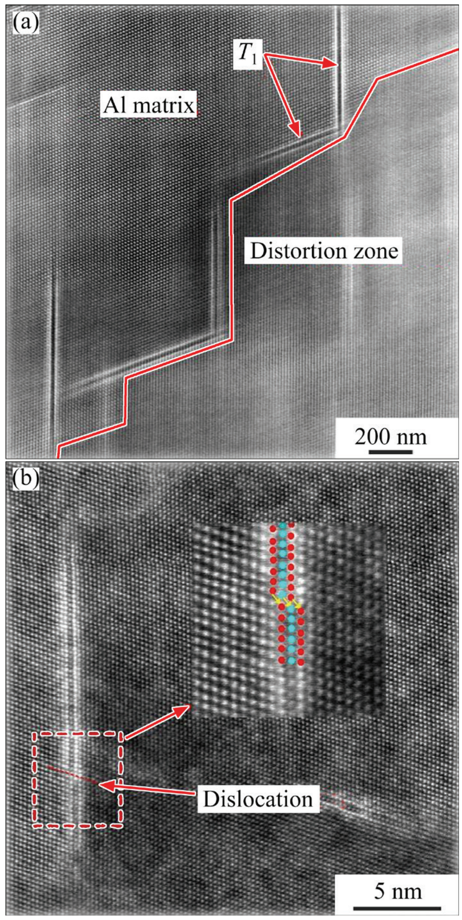

Fig. 11 TEM images of nucleation of T_1 phase along ⟨110⟩ direction (a) and sheared by dislocations (b)

4 Discussion

4.1 Effects of cold rolling pre-deformation on microstructure

It is well known that the types of precipitates in Al−Li alloys are relatively complex, and the interaction between the precipitates makes the relationship between the microstructure and properties more complicated than that of other Al alloys [18,19]. In order to further improve the comprehensive properties of the alloy, adding pre-deformation before aging becomes the focus of relevant research. A large number of dislocations can be introduced by the pre-deformation, and the dislocation density gradually increases with the increase of the pre-strain. These dislocations will affect the competitive precipitation relationship of the precipitates in the aging treatment, and then affect the precipitation behavior and the number of the precipitates [9,20]. The T_1 phase is semi-coherent with the matrix, because the interface energy and coherent strain energy of the T_1 phase are high, and the energy required for nucleation is also large, in order to reduce the nucleation energy, the T_1 phase usually nucleates preferentially on dislocations, grain boundaries, and subgrain boundaries (Fig. 11(a)) [21]. As shown in Fig. 10, when the pre-strain is 0, the number density of T_1 phase is small, but its average diameter and thickness are large, which can reach 83.6 and 3 nm, respectively. However, when the rolling pre-strain is introduced before aging, a large number of nucleation sites can be provided, and the number density of T_1 phase increases significantly. But the content of alloying elements is limited, so the size decreases gradually, as shown in Fig. 6. In addition, the strong interaction of Li−Cu and the high binding energy of Li vacancy can contribute to the precipitation and nucleation of the T_1 phase, while inhibiting the precipitation and nucleation of θ' phase. The precipitation of T_1 phase consumed a large amount of Cu atoms in the matrix, which reduced the number of Cu atoms, thereby further inhibiting the θ' precipitation [22]. However, it is worth noting that dislocations can simultaneously promote the precipitation of T_1 and θ' phases in the matrix, especially the precipitation of T_1 phase. The heterogeneous nucleation of the two precipitated phases at the dislocation is expressed by the dimensionless parameter m, and with the increase of the value of m, its effect on the nucleation and precipitation of the secondary phase can be shown by the following formula:

$$m=\frac{\Delta E_{\mathrm{V}} G b^2}{2\pi^2\sigma^2} \tag{1}$$

where ΔE_{v} is the change in volume free energy, G is the shear modulus, b is the amplitude of Burgers vector, and σ is the interface energy required to form a new surface [23,24]. The θ' phase is in a metastable state but the T_1 phase is an equilibrium phase, so the T_1 strengthening phase has a higher volume free energy [23]. The interface energy and shear modulus between T_1 and θ' phase are almost the same. Therefore, it can be known from Formula (1) that when the precipitated phase nucleates on the dislocation, the T_1 strengthening phase is preferentially precipitated during aging, and its precipitation density is much higher than that of the θ' phase, which is consistent with the results in Fig. 10. The increase in the precipitation density also shortens the distance between the strengthening phases, resulting in a decrease in the diffusion distance between solute atoms. When the precipitation phase is smaller than the critical size, it can quickly dissolve and diffuse to the nearby larger T_1 phases, providing the required Cu and Li atoms for the thickening of the T_1 phase [25]. Moreover, dislocations can also provide diffusion channels for atoms, allowing Cu atoms and Li atoms to rapidly diffuse and nucleate [26]. However, dislocation density will increase with the increase of pre-strain. Entanglement will occur when the dislocation density increases to a certain extent. In the aging process, the diffusion of solute atoms is hindered, the diffusion rate of atoms decreases, the precipitation efficiency decreases, and the number of precipitated phases decreases. In addition, when atomic diffusion efficiency is reduced, atoms can only choose to precipitate nearby, and in this case, the precipitated phase tends to coarsen preferentially.

The pre-deformation before aging can not only introduce a large number of dislocations in the matrix, but also reduce the grain size, resulting in an increase in the number of grains and grain boundaries. With the increase of pre-deformation, different degrees of distortion occur in the same grain, resulting in a certain misorientation in the same grain. When the orientation difference is 3°−15°, LAGBs will be formed inside the grain to further refine the grain. GAM reflects the size of the orientation difference between two adjacent pixels within a grain. In this experiment, the misorientation originates from the distortion caused by the external force acting on the grains. As shown in Fig. 4, the grains along the ND direction are relatively coarse in the undeformed sample, and with the increase of the pre-strain, the grain size decreases. When the stress is applied on the alloy, due to the high strength of the grain boundary, the stress is not enough to cause cracking of the grain boundary. Therefore, for the same degree of applied stress, small-size grains experience greater energy, resulting in a greater degree of distortion within grains [27]. As shown in Fig. 5, with the increase of the pre-strain, the average grain misorientation gradually increases. When the pre-strains reach 16% and 20%, the LAGBs inside the grain increase significantly, as shown in Figs. 4(e) and (f), respectively. When the pre-strain is 4%, a certain degree of distortion is generated inside the grain.

But due to the low stress level, the distortion is not sufficient to form LAGBs. As mentioned above, the T_1 phase is easy to nucleate at the subgrain boundary or in the distortion zone. Therefore, with the increase of the pre-strain, the distortion zone and LAGBs in the same grain increase, the nucleation of the T_1 phase increases, and the number density gradually increases.

4.2 Effect of pre-deformation on mechanical properties

In 2050 Al−Li alloy, the T_1 phase is the main strengthening phase, and its strengthening effect is obviously better than that of the other strengthening phases such as θ' phase [28]. There are obvious differences in the strengthening effect of different types, shapes, and sizes of precipitates [29]. NIE et al [30] studied the relationship between the strengthening effect, shape and orientation of the precipitates according to the Orowan formula listed below:

$$\Delta\tau=\frac{Gb}{4\pi\sqrt{1-v}}\cdot\frac{1}{\lambda}\ln\frac{D_{\mathrm{p}}}{r_0} \tag{2}$$

where $\Delta\tau$ is the critical shear stress increment caused by the precipitates; v is the Poisson ratio; λ is the effective distance between the precipitates; D_{p} is the average diameter of the precipitates; r_0 is the dislocation core radius. The effective distance between the precipitates can be affected by the morphology, orientation and size of the precipitates. Comparing the critical shear stress of the precipitate phases with different orientations, it can be found that the critical shear stress caused by the T_1 phase with a large length/diameter ratio is much larger than that caused by the θ' phase. Therefore, the T_1 phase is the main strengthening phase. When the dislocation encounters a high density of T_1 phases during the movement, a large number of dislocation loops can be produced, resulting in the accumulation of dislocations. In addition, the dislocation loops shorten the distance between the precipitates and increase the resistance of dislocation movement, thereby strengthening the alloy. However, since the T_1 phase is a brittle phase, the dispersing effect of T_1 relative to co-planar slip is not obvious and difficult to improve the plasticity of the alloy.

T_1 precipitate is originally considered as a non-shearable particle [31,32]. However, recent researches [33,34] revealed that T_1 phase plays a role as a shearable precipitate that can be sheared by dislocations but only once at the same location (Fig. 11). Therefore, the T_1 phase should be separated into two types (shearable T_1 phase and non-shearable T_1 phase), which affect mechanical properties of 2050 Al−Li alloy. However, the interaction mechanism between the T_1 phase and the dislocation depends on the thickness of T_1 phase. When the thickness of the T_1 phase is less than 3 nm, it can be sheared by dislocations (Fig. 11(b)), but it becomes non-shearable when the thickness is greater than 3 nm [17]. In addition, DORIN et al [34] used HRTEM and found that the sliding surface of the T_1 strengthening phase could not be dissected again after one dissection. The precipitation strengthening effect and related parameters of the T_1 strengthening phase are as follows:

$$\Delta\tau=D^2N^{1/2}t^{-3/2} \tag{3}$$

where D is the diameter of the T_1 strengthening phase, N is the number density of the T_1 strengthening phase, and t is the thickness of the T_1 phase. It can be seen from Formula (3) that the diameter and density of T_1 phase are proportional to the strength, and the thickness of T_1 phase is inversely proportional to the strength. During the tensile deformation process, a stress field appears near the T_1 phase, increasing the minimum shear stress to drive the dislocation. When the dislocation shears the T_1 phase, the dislocation can produce a large bending angle and a large thread tension. The distribution of the secondary phase in the matrix determines the linear tension of the dislocation, and the shorter the distance between the second phases, the greater the linear tension of the dislocation. Therefore, when the T_1 strengthening phase has a higher number density, the precipitated phase can pin the dislocations better, thereby improving the yield strength [34,35]. As shown in Figs. 6 and 10, with the increase of the pre-deformation strain, the number density of T_1 precipitates gradually increased, the distance between the precipitates gradually decreased, and the resistance to dislocations gradually increased, so the strength of the alloy gradually increased. Moreover, according to related research [36], when the deformation increased to a critical value, the number of channels due to dislocation entanglement decreased and the number of T_1 phases decreased. Therefore, when the pre-strain was greater than 16%, the number of precipitation phases decreased, the distance between the precipitation phases increased, the hindering effect on dislocations decreased, and hence, the strength of the alloy decreased.

5 Conclusions

(1) With the increase of pre-strain, the strength of the alloy first increased and then decreased. When the pre-strain is 16%, the strength of alloy reaches the maximum value, σ_b and σ_s are 584 and 568 MPa, respectively, and the elongation is 8.6%.

(2) Adding pre-deformation before aging can not only introduce dislocations in the matrix, but also change the grain structure of the alloy, thereby promoting precipitation. However, when the pre-deformation strain reaches 20%, the dislocation is entangled, resulting in a decrease in nucleation sites and the number density of the T_1 phase.

(3) The T_1 phase is the main strengthening phase in the 2050 alloy, and the greater the number density of the T_1 phase is, the greater the linear tension generates when the dislocation shears the T_1 phase, and the corresponding strength is higher.

(4) The pre-deformation results in severe deformation of grain along the ND direction, the grain size decreases along the ND direction and the internal distortion increases, which promotes the precipitation.

CRediT authorship contribution statement

Yao LI: Execute the experimental protocol and write the paper; **Guo-fu XU:** Implement the feasibility of the experimental method and monitor the progress of the experiment; **Hai-guang QIAO:** Prepare transmission specimens; **Shi-chao LIU:** Test mechanical properties; **Xiao-yan PENG:** Jointly formulate the experimental plan and revise the specification.

Declaration of competing interest

No conflict of interest exits in the submission of this manuscript, and manuscript is approved by all authors for publication. I would like to declare on behalf of my co-authors that the work described was original research that has not been published previously, and not under consideration for publication elsewhere, in whole or in part.

Data availability

The raw/processed data required to reproduce these findings cannot be shared at this time as the data also form part of an ongoing study.

Acknowledgments

This investigation was financially supported by the National Key Research and Development Program of China (No. 2018YFB2001801), the National Key Project of Research and Development Plan (No. 2021YFC1910505), the Hunan Provincial Natural Science Foundation of China (No. 2020JJ5742), and the Key Research and Development Program of Guangdong Province, China (No. 2020B010186002).

References

[1] WILLIAMS J C, STARKE E A Jr. Progress in structural materials for aerospace systems [J]. Acta Materialia, 2003, 51: 5775−5799.

[2] DURSUN T, SOUTIS C. Recent developments in advanced aircraft aluminium alloys [J]. Materials & Design, 2014, 56: 862−871.

[3] GUPTA R K, NAYAN N, NAGASIREESHA G, SHARMA S C. Development and characterization of Al−Li alloys [J]. Materials Science and Engineering A, 2006, 420: 228−234.

[4] EL-ATY A A, XU Y, GUO X Z, ZHANG S H, MA Y, CHEN D Y. Strengthening mechanisms, deformation behavior, and anisotropic mechanical properties of Al−Li alloys [J]. Journal of Advanced Research, 2018, 10: 49−67.

[5] RIOJA R J, LIU J. The evolution of Al−Li base products for aerospace and space applications [J]. Metallurgical and Materials Transactions A, 2012, 43: 3325−3337.

[6] FRIDLYANDER I N, GRUSHKO O E, SHAMRAI V F, KLOCHKOV G G. High-strength structural silver-alloyed under-density Al−Cu−Li−Mg alloy [J]. Metal Science and Heat Treatment, 2007, 49: 279−283.

[7] ANTIPOV V V, KOLOBNEV N I, KHOKHLATOVA L B. Advancement of Al−Li alloys and of multistage modes of their heat treatment [J]. Metal Science and Heat Treatment, 2014, 55: 459−465.

[8] SHAMRAI V F, GRUSHKO O E, LAZAREV E M, GORDEEV A S, TIMOFEEV V N. X-ray diffraction study of the structural evolution in a grade 1469 (Al−Cu−Li) alloy during the production of hot-rolled sheets [J]. Russian Metallurgy, 2008, 3: 245−251.

[9] RODGERS B I, PRANGNELL P B. Quantification of the influence of increased pre-stretching on microstructure−strength relationships in the Al−Cu−Li alloy AA2195 [J]. Acta Materialia, 2016, 108: 55−67.

[10] DORIN T, DESCHAMPS A, GEUSER F D, SIGLI C. Quantification and modelling of the microstructure/strength relationship by tailoring the morphological parameters of the T_1 phase in an Al−Cu−Li alloy [J]. Acta Materialia, 2014, 75: 134−146.

[11] GABLE B M, ZHU A W, CSONTOS A A, STARKE E A Jr. The role of plastic deformation on the competitive microstructural evolution and mechanical properties of a novel Al−Li−Cu−X alloy [J]. Journal of Light Metals, 2001, 1: 1−14.

[12] ISTOMIN-KASTROVSKII V V, SHAMRAI V F, GRUSHKO O E, KLOCHKOVA Y Y, RYAZANTSEVA M A. Effect of silver, magnesium, and zirconium additions on aging of a V1469 alloy (Al−Cu−Li system) [J]. Russian Metallurgy, 2010, 9: 819−823.

[13] CASSADA W A, SHIFLET G J, STARKE ET E A Jr. The effect of plastic deformation on T1 precipitation [J]. Colloques, 1987, 48: 397−406.

[14] XIE B X, HUANG L, XU J H, SU H L, ZHANG H P, XU Y K, LI J J, WANG Y. Effect of the aging process and pre-deformation on the precipitated phase and mechanical properties of 2195 Al−Li alloy [J]. Materials Science and Engineering A, 2022, 832: 142394.

[15] DUAN S W, GUO F Q, WU D T, WANG T, TSUCHIYA T, MATSUDA K J, ZOU Y. Influences of pre-rolling deformation on aging precipitates and mechanical properties for a novel Al−Cu−Li alloy [J]. Journal of Materials Research and Technology, 2021, 15: 2379−2392.

[16] DONNADIEU P, SHAO Y, GEUSER F D, BOTTON G A, LAZAR S, CHEYNET M, BOISSIEU M D, DESCHAMPS A. Atomic structure of $T1$ precipitates in Al−Li−Cu alloys revisited with HAADF-STEM imaging and small-angle X-ray scattering [J]. Acta Materialia, 2011, 59: 462−472.

[17] SHERCLIFF H R, ASHBY M F. A process model for age hardening of aluminium alloys—II. Applications of the model [J]. Acta Metallurgica et Materialia, 1990, 38: 1803−1812.

[18] CHEN Z W, ZHAO K, FAN L. Combinative hardening effects of precipitation in a commercial aged Al−Cu−Li−X alloy [J]. Materials Science and Engineering A, 2013, 588: 59−64.

[19] DENG Y, PENG B, XU G F, PAN Q L, YE R, WANG Y J, LU L Y, YIN Z M. Stress corrosion cracking of a high-strength friction-stir-welded joint of an Al−Zn−Mg−Zr alloy containing 0.25 wt.% Sc [J]. Corrosion Science, 2015, 100: 57−72.

[20] XIN T Z, TANG S, JI F, CUI L Q, HE B B, LIN X, TIAN X L, HOU H, ZHAO Y H, FERRY M. Phase transformations in an ultralight BCC Mg alloy during anisothermal ageing [J]. Acta Materialia, 2022, 239: 118248.

[21] HU L B, ZHAN L H, LIU Z L, SHEN R L, YANG Y L, MA Z Y, LIU M, LIU J, YANG Y G, WANG X. The effects of pre-deformation on the creep aging behavior and mechanical properties of Al−Li−S4 alloys [J]. Materials Science and Engineering A, 2017, 703: 496−502.

[22] MA P P, ZHAN L H, LIU C H, WANG Q, LI H, LIU D B, HU Z G. Pre-strain-dependent natural ageing and its effect on subsequent artificial ageing of an Al−Cu−Li alloy [J]. Journal of Alloys and Compounds, 2019, 790: 8−19.

[23] LI J F, YE Z H, LIU D Y, CHEN Y L, ZHANG X H, XU X Z, ZHENG Z Q. Influence of pre-deformation on aging precipitation behavior of three Al−Cu−Li alloys [J]. Acta Metallurgica Sinica (English Letters), 2017, 30: 133−145.

[24] WANG J X, LIU Q, LI J F, CHEN Y L, ZHANG X H, XU X Z, ZHENG Z Q. Effect of aging treatment on mechanical properties and microstructures of super-high strength Al−Cu−Li−X alloy [J]. Journal of Central South University (Science and Technology), 2018, 49: 794−801. (in Chinese)

[25] YOSHIMURA R, KONNO T J, ABE E J, HIRAGE K J. Transmission electron microscopy study of the evolution of precipitates in aged Al−Li−Cu alloys: The θ' and T1 phases [J]. Acta Materialia, 2003, 51: 4251−4266.

[26] DESCHAMPS A, FRIBOURG G, BRECHET Y. In situ evaluation of dynamic precipitation during plastic straining of an Al−Zn−Mg−Cu alloy [J]. Acta Materialia, 2012, 60: 1905−1916.

[27] ZHANG P, LIU J L, GAO Y R, LIU Z H, MAI Q Q. Effect of heat treatment process on the micro machinability of 7075 aluminum alloy [J]. Vacuum, 2023, 207: 111574.

[28] NOBLE B, THOMPSON G E. $T_1(Al_2CuLi)$ precipitation in aluminium–copper–lithium alloys [J]. Metal Science Journal, 2013, 9: 164−174.

[29] HUANG J C, ARDELL A J. Addition rules and the contribution of δ' precipitates to strengthening of aged Al−Li−Cu alloys [J]. Acta Metallurgica, 1988, 36: 2995−3006.

[30] NIE J F, MUDDLE B C, POLMEAR I J. The effect of precipitate shape and orientation on dispersion strengthening in high strength aluminium alloys [J]. Materials Science Forum, 1996: 1257−1262.

[31] BLANKENSHIP C P Jr, HORNBOGEN E, STARKE E A Jr. Predicting slip behavior in alloys containing shearable and strong particles [J]. Materials Science and Engineering A, 1993, 169: 33−41.

[32] GAO C, MA Y, TANG L Z, WANG P, ZHANG X. Microstructural evolution and mechanical behavior of friction spot welded 2198-T8 Al−Li alloy during aging treatment [J]. Materials & Design, 2017, 115: 224−230.

[33] CSONTOS A A, STARKE E A. The effect of inhomogeneous plastic deformation on the ductility and fracture behavior of age hardenable aluminum alloys [J]. International Journal of Plasticity, 2005, 21: 1097−1118.

[34] DORIN T, GEUSER F D, LEFEBVRE W, SIGLI C, DESCHAMPS A. Strengthening mechanisms of T1 precipitates and their influence on the plasticity of an Al−Cu−Li alloy [J]. Materials Science and Engineering A, 2014, 605: 119−126.

[35] DUAN S Y, WU C L, GAO Z, CHA L M, FAN T W, CHEN J H. Interfacial structure evolution of the growing composite precipitates in Al−Cu−Li alloys [J]. Acta Materialia, 2017, 129: 352−360.

[36] LU Y L, JIAN W, LI X, YI C, XU W. Effect of pre-deformation on the microstructures and properties of 2219 aluminum alloy during aging treatment [J]. Journal of Alloys and Compounds, 2016, 699: 1140−1145.

预变形量对 2050 Al−Li 合金显微组织和力学性能的影响

李 耀[1]，徐国富[1,2]，乔海光[1]，刘时超[1]，彭小燕[1]

1. 中南大学 材料科学与工程学院，长沙 410083；
2. 中南大学 有色金属材料科学与工程教育部重点实验室，长沙 410083

摘 要：研究经不同轧制预变形处理(0~20%)后 2050 Al−Li 合金 T8 时效状态的显微组织演变和力学性能。通过透射电子显微镜(TEM)和扫描电子显微镜(SEM)对其显微组织进行表征。结果表明：随着预变形量的增加，晶粒尺寸沿 ND 方向显著变小，晶内畸变增大。位错等的缠结为 T_1 相的析出提供了大量的形核位点。这导致析出相数量增多，析出相之间的距离缩小，从而提高了对位错运动的阻碍作用和合金强度。当预变形量为 16%时，T_1 相数量密度和合金强度最高(屈服强度和抗拉强度分别达到 568 和 584 MPa，伸长率为 8.6%)；当预变形量进一步增加到 20%时，由于位错缠结，原子扩散通道减少，T_1 相数量的减少最终导致合金强度降低。

关键词：2050 铝锂合金；轧制预变形；T_1 相；显微组织；力学性能

(Edited by Wei-ping CHEN)